Title
Comparison With Global Soil Radiocarbon Observations Indicates Needed Carbon Cycle Improvements in the E3SM Land Model

Journal
Journal of Geophysical Research Biogeosciences, 124(5)

ISSN
2169-8953

Authors
Chen, Jinsong
Zhu, Qing
Riley, William J
et al.

Publication Date
2019-05-01

DOI
10.1029/2018jg004795

Peer reviewed

Comparison With Global Soil Radiocarbon Observations Indicates Needed Carbon Cycle Improvements in the E3SM Land Model

Jinsong Chen[1], Qing Zhu[1], William J. Riley[1], Yujie He[2], James T. Randerson[2], and Susan Trumbore[2]

Correspondence to: J. Chen, jchen@lbl.gov

Abstract

We evaluated global soil organic carbon (SOC) stocks and turnover time predictions from a global land model (ELMv1-ECA) integrated in an Earth System Model (E3SM) by comparing them with observed soil bulk and $\Delta^{14}C$ values around the world. We analyzed observed and simulated SOC stocks and $\Delta^{14}C$ values using machine learning methods at the Earth System Model grid cell scale (~200 km). In grid cells with sufficient observations, the model provided reasonable estimates of soil carbon stocks across soil depth and $\Delta^{14}C$ values near the surface but underestimated $\Delta^{14}C$ at depth. Among many explanatory variables, soil albedo index, soil order, plant function type, air temperature, and SOC content were major factors affecting predicted SOC $\Delta^{14}C$ values. The influences of soil albedo index, soil order, and air temperature were primarily important in the shallow subsurface (≤30 cm). We also performed sensitivity studies using different vertical root distributions and decomposition turnover times and compared to observed SOC stock and $\Delta^{14}C$ profiles. The analyses support the role of vegetation in affecting soil carbon turnover, particularly in deep soil, possibly through supplying fresh carbon and degrading physical-chemical protection of SOC via root activities. Allowing for grid cell-specific rooting and decomposition rates substantially reduced discrepancies between observed and predicted $\Delta^{14}C$ values and SOC content. Our results highlight the need for more explicit representation of roots, microbes, and soil physical protection in land models.

Plain Language Summary

Quantifying feedbacks between the terrestrial carbon cycle and climate is important for understanding climate change. Among many factors that control terrestrial carbon cycle responses to climate, soil organic carbon (SOC) dynamics are particularly important, although highly uncertain. In addition to SOC stocks, radiocarbon is an important observational constraint for land model predictions. We evaluated, against worldwide observations of SOC stocks and radiocarbon, predictions from a new land model used for climate change analyses. We analyzed differences between model predictions and observations using a machine learning method at a large grid cell scale (~200 km). Among many explanatory variables, soil albedo index, soil order, plant function type, air temperature, and SOC densities were major factors affecting predicted SOC radiocarbon values. The influences of soil albedo index, soil order, and air temperature were primarily important for topsoil. Our sensitivity analysis highlights the role of plant root

activity in affecting soil carbon turnover, particularly in deep soil, possibly through supplying fresh carbon and degrading physical-chemical protection of SOC. Allowing for grid cell-specific rooting and decomposition rates substantially reduced discrepancies between observed and predicted values. Our results highlight the need for more explicit representation of roots, microbes, and soil physical protection in land models.

1 Introduction

Global land models integrated in Earth System Models (ESMs) have been used to quantify feedbacks between the terrestrial carbon cycle and climate (Friedlingstein et al., 2014). Among many factors affecting terrestrial carbon cycle responses to climate, soil organic carbon (SOC) turnover is particularly important (Bloom et al., 2016; Carvalhais et al., 2014) but substantially underestimated in Coupled Model Intercomparison Project Phase 5 ESMs. As demonstrated by He et al. (2016), systematic errors in the representation of soil organic matter (SOM) dynamics could lead to very large uncertainties in the ability of soils to buffer expected effects of climate change.

Developing model representations of vertically resolved SOC stocks and turnover at multiple spatial scales has proven challenging because of uncertainties in mechanistic representations (Ahrens et al., 2015; Riley et al., 2014; Schmidt et al., 2011), parameter estimation (Luo et al., 2016), system characterization (e.g., soil properties and vegetation type) (Mathieu et al., 2015), and climate forcing (Campo & Merino, 2016). Although several observationally constrained and spatially resolved estimates of global SOC stocks are available (Hengl et al., 2014), estimating in situ SOC dynamics from observations over decadal to centennial time scales remains challenging. Existing methods include combining observed SOC stock and aboveground and belowground net primary production estimates (Liski et al., 2006), intact soil core incubations (Thomsen et al., 2003), ^{13}C tracer studies (Torn et al., 1997), and soil radiocarbon (^{14}C) observations. Among those methods, SOC $\Delta^{14}C$ profiles provide the most direct constraints on site (Ahrens et al., 2015; Dwivedi et al., 2017; Torn et al., 1997) to global-scale model (Koven et al., 2013) estimates of soil carbon dynamics in a vertically explicit manner.

Comparing site-scale soil measurements to ESM-scale model predictions presents a range of challenges, including biases and scale mismatches in system characterization and climate forcing (Mekonnen et al., 2016; Schwalm et al., 2010). The first main challenge results from horizontal scale discrepancies between the site and the model. Site measurements are typically representative of horizontal spatial scales on the order of 1 to 100 m, while ESM land models have horizontal resolutions of tens to hundreds of kilometers. Therefore, ESM SOC $\Delta^{14}C$ predictions attempt to represent average values across each model grid cell but not necessarily observations at a particular site across a heterogeneous landscape. This mismatch in spatial scales makes a direct comparison between site-scale

measurements and ESM-scale predictions potentially misleading, for example, due to the spatial heterogeneity of SOC $\Delta^{14}C$ values and their dependence on site-specific factors. We note that this challenge exists for many features of ESM land model predictions (Jiang et al., 2015; Mishra & Riley, 2015).

The second main challenge is that site-scale measurements and ESM-scale predictions have different sources and characteristics of uncertainty. For site measurements, the primary source of uncertainty is measurement errors, including errors in SOC $\Delta^{14}C$ measurements (e.g., associated with the incomplete sampling of spatial heterogeneity) and errors in associated variables required for interpretation (e.g., bulk density and SOC concentration). However, land models incorporate many sources of uncertainty, including structural, system characterization, numerical implementation errors, and parameterization (e.g., Luo et al., 2016). Characterizing those uncertainties and their effects on model predictions is difficult.

Recognizing those challenges, we first compared site measurements (i.e., 671 site-level vertically resolved SOC $\Delta^{14}C$ observations) with predictions from a global land model (ELMv1-ECA; see section 2) at the grid cell scale. A small portion of the site measurements has been used by some researchers to calibrate site-level land models for understanding processes that control SOM dynamics (Ahrens et al., 2015; Dwivedi et al., 2017; Jenkinson & Coleman, 2008). However, at the global scale, to our knowledge, the ability to simulate SOC $\Delta^{14}C$ values and vertical profiles currently exist in only two ESM land models, that is, Community Land Model (CLM; Koven et al., 2013) and ELMv1-ECA (Zhu et al., 2017). ELMv1-ECA, which is integrated in the ESM Energy Exascale Earth System Model (E3SM), was derived from CLM4.5 and shares aspects of its belowground Century-based (Parton et al., 1993) soil carbon module, although the aboveground carbon cycle dynamics and connections with belowground processes (e.g., nutrient dynamics and competition) have been substantially changed (see section 2). We then employed statistical models to characterize limitations of ELMv1-ECA and provided suggestions for possible improvements. Our goals are to identify dominant factors affecting discrepancies between simulated and observed SOC $\Delta^{14}C$ values, identify potential model process representations responsible for these biases, and provide guidance for future model development.

2 Methods

2.1 Site Observations and ESM-Scale Data

We used a recently assembled global SOC $\Delta^{14}C$ observational data set from 671 sites (He et al., 2016; Mathieu et al., 2015; Figure 1) for our analysis. Since the soils represented in the data set were collected between 1900 and 2013, we first “normalized” them to year 2000 at each ESM grid given the measured atmospheric $\Delta^{14}C$ as input, using the approach developed by He et

al. (2016). The spatial density of observational sites varies widely across the globe, with relatively poor coverage in Africa, China, and Eastern Europe. Although the data sets listed a wide range of properties, many of them were measured only at a small number of sites. For this study, we chose commonly measured properties at the 671 sites: vertically resolved SOC stock, elevation, soil order, mean annual temperature, mean annual precipitation, Whittaker's biome types, total SOC stock, soil bulk density, and percentage of carbon (more details of the measurements are given in He et al., 2016). In addition, to maximize the total number of sites available for comparison, we combined measurements from organic and mineral soil horizons based on the measurement depth because the current model does not explicitly resolve their differences.

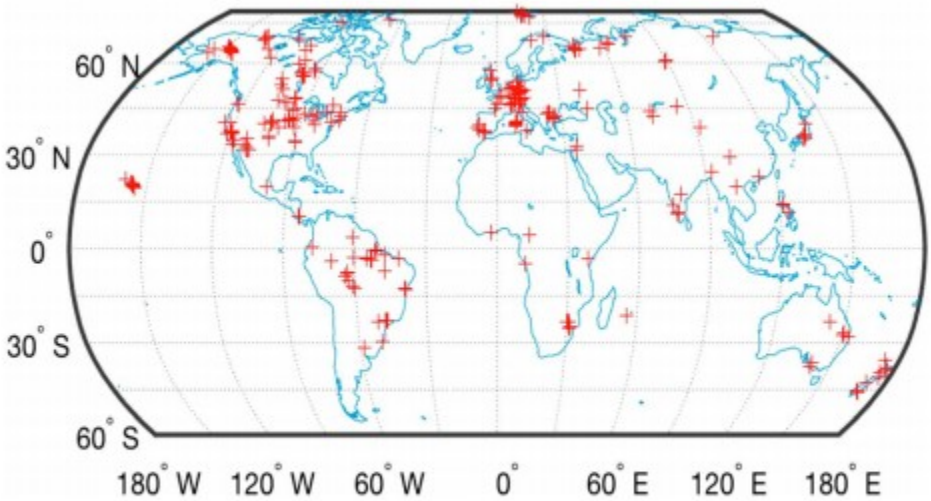

Figure 1. Locations of global soil radiocarbon observation sites (red plus signs). There are 671 sites in total around the global.

We used a data-driven approach in this analysis to analyze data at the ESM scale. Even though some parameters seem mechanistically unrelated at the local scale, it is possible for them to be associated with each other at the ESM scale through some compound hidden factors. We included all available ESM-scale information (or forcing data) in this study to identify useful information to improve mechanistic understanding. The ESM-scale data are primarily surface and near-surface information, and they came from different sources. For this study, we only used those that are as input to our model. Specifically, they include air and soil temperature, precipitation (or rainfall), slope, elevation standard deviation, clay content, SOM density (SOMD), soil albedo index, soil order, and plant function types (PFTs). We obtained the temperature and rainfall data from CRUNCEP Version 7 data set (Viovy, 2018) and the slope and elevation standard deviation from HYDRO1k (Verdin & Greenlee, 1996). We extracted clay content and SOMD data from Global Soil Data Task (Task, 2000), soil albedo index and soil order data from a global surface data set (Lawrence & Chase, 2007), and global PFTs based

on Lawrence and Chase (2010). For soil order and PFTs, at those grid cells where site measurements are available, we directly used the data from He et al. (2016). Calculating soil albedo index involved fitting soil reflectance values at each grid for each month to find values that would reproduce the same average snow-free surface albedo as were observed by Moderate Resolution Imaging Spectroradiometer (MODIS) at local solar noon on the middle day of the month (Lawrence & Chase, 2007).

2.2 ELMv1-ECA Model

2.2.1 Model Structure

The development of ELMv1-ECA started from CLM4.5BGC (Koven et al., 2013), which represents vertically resolved soil Biogeochemistry (BGC) based on the Century model (Parton et al., 1993) including decomposition, soil O_2 and its effects on decomposition, plant inputs, and soil nitrogen dynamics. ELMv1-ECA added several features that affect C inputs to soil and SOC dynamics. Briefly, the relevant changes for the current work include the following: (a) incorporation of a prognostic phosphorus cycle based on Wang et al. (2007); (b) a new approach to represent nutrient competition between plants, microbes, and mineral surfaces based on the equilibrium chemistry approximation (ECA) (Tang & Riley, 2013; Zhu et al., 2016, 2017); (c) dynamic leaf stoichiometry that affects photosynthesis (Ghimire et al., 2016; Walker et al., 2014); and (d) dynamic C, N, and P allocation within the plant based on Friedlingstein et al. (1999), which considers light, water, soil nitrogen, and phosphorus stresses.

Although the basic structures in ELMv1-ECA and CLM4.5 for soil ^{12}C and ^{14}C dynamics are the same, there are differences between the models in representing terrestrial nutrient cycles, and therefore constraints on SOC dynamics. Specifically, CLM4.5 represents carbon and nitrogen interactions with the relative demand hypothesis, which limits plant and soil nitrogen uptake rates based on competitors' relative demands. In contrast, ELMv1-ECA constrains carbon, nitrogen, and phosphorus interactions using the ECA competition hypothesis (Riley et al., 2018). ECA partitions available soil nutrients to multiple nutrient consumers based on their competitive traits (e.g., maximum uptake rates and affinities) (Zhu et al., 2017).

2.2.2 Numerical Simulation

We simulated vertical profiles of SOC $\Delta^{14}C$ values globally using ELMv1-ECA on 1.9° × 2.5° grids. For this study, we used the 10 layers of biogeochemically active soil to a depth of 380 cm with exponentially increasing thicknesses from 1.6 to 90 cm with higher spatial resolution near the surface (Koven et al., 2013).

The model was driven by CRUNCEP reanalysis meteorological forcing (Harris et al., 2014), including temperature, precipitation, wind speed, humidity, radiation, and air pressure. Model simulations first ran to preindustrial (1850) equilibrium condition with a two-step process using prescribed PFT

distributions (K.W. Oleson & Bonan, 2000) and constant atmospheric CO_2 concentration (285 ppm). In the first step, the model ran for 1,000 years with “accelerated soil decomposition,” which is an approach that increases the turnover time of the soil carbon pools (slow turnover pool and passive pool) by 15 and 675 times (Koven et al., 2013). This approach ensures that both the soil carbon bulk and ^{14}C pools have equilibrated. The atmospheric radiocarbon content during the spin-up is held constant at 0‰ (Koven et al., 2013), although there is evidence from tree rings that atmospheric concentrations over the past 20,000 years were ^{14}C enriched compared to present day (Reimer et al., 2013). Given the computational cost of ELMv1-ECA, it is not possible to run a simulation for 20,000 years to account for the history. However, analysis with a simple first-order decay SOC model indicates that the $\Delta^{14}C$ bias associated with the assumption of ignoring this atmospheric enrichment is between a few per mil near the surface and ~50‰ at depth; we will discuss the impact of this potential bias in section 5 below.

The second step is a 200-year “regular spin-up” with baseline soil decomposition rates to produce the 1850 equilibrated state. The model output at the end of the spin-up was then used to initialize the model for the 1850–2000 transient simulation with diagnostic atmospheric CO_2 concentrations from Mauna Loa Observatory (Masarie & Tans, 1995), nitrogen and phosphorus deposition (Lamarque et al., 2005; Mahowald et al., 2008), and atmospheric $\Delta^{14}C$ values, which include the nuclear weapons testing sources (“bomb spike”) (Levin et al., 2010). The atmospheric $\Delta^{14}C$ values are taken in those simulations to be spatially uniform.

2.2.3 Sensitivity Analysis

In addition to the baseline simulation, we also conducted modeling experiments to explore the sensitivity of ELMv1-ECA-simulated SOC and $\Delta^{14}C$ values to several factors. Based on previous work (e.g., Dwivedi et al., 2017; Koven et al., 2013), vertically resolved SOC $\Delta^{14}C$ values are sensitive to both vertical rooting profiles (and therefore fresh carbon inputs) and SOC decomposition rates. In ELMv1-ECA (as in CLM4.5), the z_τ parameter controls the vertical decline in soil decomposition rates. We therefore performed sensitivity analyses to rooting profiles (Jackson et al., 1997; Zeng, 2001) and z_τ values (0.2, 0.35, 0.5, 0.65, and 0.8 m). A lower z_τ value implies lower SOC decomposability with increasing depth (Koven et al., 2013). The protocols for spin-up and transient simulations are identical to the baseline simulation. Our objective with these analyses is to gain insights into the relative importance of input versus turnover vertical profiles on SOC ^{14}C dynamics.

2.3 Methods for Comparison

Ideally, the model should be forced with characterization and climate forcing measurements at the site scale so that scale discrepancies could be minimized and direct comparisons with measurements could be made.

Unfortunately, this approach is impractical for this study due to the lack of local information across the 671 sites. As discussed above, comparisons between site-scale observations and ESM-scale model predictions face several problems because of scale mismatch. Since direct comparisons with model predictions forced by site-level data are not possible in this case, we made comparisons by arithmetic averaging of site observations at each depth interval measured within an ESM grid cell. As noted above, observational studies were often designed to maximize spatial heterogeneity to evaluate mechanistic controls, rather than to provide accurate large-scale estimates. An example of this potential problem is from site 21 (Hawaiian Islands; see Figure 2), where the oldest profiles are not spatially representative of the entire Hawaiian Islands. Although we are unable to address these shortcomings here, they motivate the need for more observations specifically designed to provide accurate spatial averages.

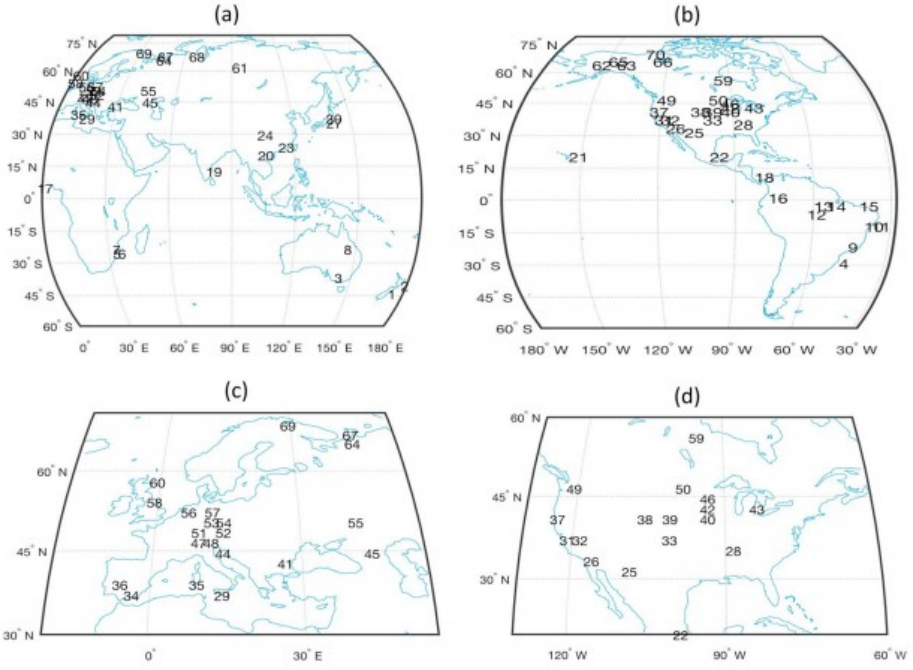

Figure 2. Locations of 70 grid cells used in the ESM-scale comparison: (a) Eastern Hemisphere, (b) Western Hemisphere, (c) details of the upper-left regions on the Eastern Hemisphere, and (d) details of the middle regions of the Western Hemisphere.

2.3.1 Statistical Approaches for Comparisons

Characterization of the spatial variability of radiocarbon requires careful experimental design as done by Schrumpf et al. (2011) for plot-scale data acquisitions. At the ESM scale, however, data acquisition at sufficiently fine scales would be prohibitive. Although current site observations were often linked to studies (e.g., chronosequences) that maximize differences to enhance process understanding, we hope they provide information on the spatial variability of the true values. We upscaled the site measurements to the ESM scale using arithmetic average and obtained values at 70 ESM grid cells (Figure 2), each of which includes at least three observations for

comparison to ELMv1-ECA predictions. We chose to use simple averaged values in this study to reduce possible biases. Since we typically have a small number of samples within each ESM grid cell and we do not know their true statistical distributions, we use bootstrap methods (Efron & Tibshirani, 1993) to calculate the sample mean and the associated standard errors. After upscaling, we investigated relationships between the averaged values and the model predictions as functions of multiple other factors using a machine learning method, which will be detailed below.

Let x_{ij}^{s} be the *j*th site measurement within the *i*th grid cell, $i \in S$ and $j \in A_i$, where S denotes the index set of all the grids that include at least three site measurements, and A_i is an index set of all the sites within the *i*th grid cell. Let $\mathrm{avg}\left(x_{ij}^{s}\right)$ and x_i^{mod} be the arithmetic average of individual measurements and model predictions within the grid cell, respectively. Since we do not have a large number of site measurements at each grid cell to reliably derive an underlying probability distribution, we assume those measurements have Gaussian distribution. Thus, we have

$$x_{ij}^{s} = \mathrm{avg}\left(x_{ij}^{s}\right) + \varepsilon_{ij}^{s}, \qquad \text{where } \varepsilon_{ij}^{s} \sim N\left(0, \sigma_i^2\right). \quad (1)$$

Ideally, the average $\mathrm{avg}\left(x_{ij}^{s}\right)$ should be strongly correlated to the model prediction x_i^{mod}. However, because of the spatial variability of $\Delta^{14}C$ values and the limited sample size within grid cells, they are often very different. The discrepancies may depend on many large- and small-scale factors. Identifying those factors and understanding their dependencies may provide useful information on improving model formulations and parameters, as well as guidance for further collection of site measurements.

We compared site-scale measurements to ESM-scale model predictions using a statistical approach. In the approach, we considered the differences between the averaged observations ($\mathrm{avg}\left(x_{ij}^{s}\right)$) and predicted values (x_i^{mod} (i.e., residuals) as dependent variables and fit them as functions of many available large-scale factors:

$$\left[\mathrm{avg}\left[x_{ij}^{s}\right] - x_i^{\mathrm{mod}}\right] \sim G(\text{large-scale factors}), \quad i \in S, \quad (2)$$

where G represents fitting functions and the other variables are defined above. We generally expect the numerical model will provide good estimates of the mean observations at the ESM scale and variations of the observed and predicted data sets are of a similar order. If one of the variations is substantially larger than another one, this approach may mainly fit the effects of the variable with the larger variations.

The goal of this analysis is to identify important factors that affect discrepancies at the ESM scale. The results may provide information on mechanistic representations of processes related to those ESM-scale factors.

It is possible that the discrepancies are mainly caused by the inaccuracy of input parameters at those scales. In this case, we need to improve the accuracy of the input data.

2.3.2 Machine Learning Method for Data Analysis

We use a tree-based ensemble machine learning method called random forests (Breiman, 2001) to perform nonlinear statistical analysis described in equation 2. Random forests is a substantial modification of “bootstrap aggregating” (also known as bagging) (Breiman, 1996), which is a technique for reducing variance in classification or regression predictions. Trees are ideal candidates for bagging because they can capture complex interaction structures in the data and they typically have large variance and low bias (Hastie et al., 2009). For regression, we first fitted the same regression tree many times to the bootstrap-sampled version of training data and then averaged their results (Hastie et al., 2009). However, simply rerunning the same learning algorithm on different subsets of the data can cause highly correlated predictors, limiting the amount of variance reduction. The random forests approach tries to decorrelate the base learner by learning trees based on randomly chosen subsets of input variables, as well as a randomly chosen subset of data cases. As a result, random forests methods often have outstanding predictive accuracy and have been widely used in many applications (Murphy, 2012). Random forests is particularly useful when input variables are correlated and the number of training data is relatively small compared to the number of inputs.

Although the goal of many applications of random forests is to obtain accurate predictions from trained models, we here focus on identifying main factors that affect the discrepancies between observed and simulated data. We set the number of trees for random forests as 1,000, which is quite large. Similar to Klueter et al. (2015), we calculated *p* value metrics with 2,000 permutations using the R package “rfPermute” developed by Archer (2016), under the null hypothesis that the tested variable is not important. If the calculated *p* value is less than a preset critical level (i.e., 0.1), we reject the null hypothesis and consider the factor to be statistically significant under the critical level.

3 Results

3.1 Direct Comparison at the ESM Scale

We first compared the averaged site $\Delta^{14}C$ measurements over grid cells with ELMv1-ECA predictions at locations with measurements available down to 100-cm depth (Figures 2a–2d). This analysis provides a general idea of how observed and simulated $\Delta^{14}C$ values are compared. Figure 3 shows the comparisons at depths of 10, 30, 50, 70, and 100 cm. The site indices are sorted from lowest to highest latitudes (i.e., increasing from south to north). We restricted the analysis to grid cells where at least three site-level observations exist for that particular depth, resulting in a decreasing number

of sites as depth increased (i.e., 59, 53, 49, 39, and 27 sites for depths of 10, 30, 50, 70, and 100 cm, respectively). We used linear interpolation to estimate values at those depths where observations and model predictions were not aligned. The model predictions were generally consistent with the mean site measurements at each depth, but uncertainties in the averaged site measurements were large and the root mean square discrepancies increased with increasing depths (i.e., 134‰, 137‰, 139‰, 157‰, and 157‰ for depths 10, 30, 50, 70, and 100 cm, respectively). In addition, the model was compared poorly with observations for site indices above 60, which correspond to sites with latitudes higher than 56°N (Figure 2).

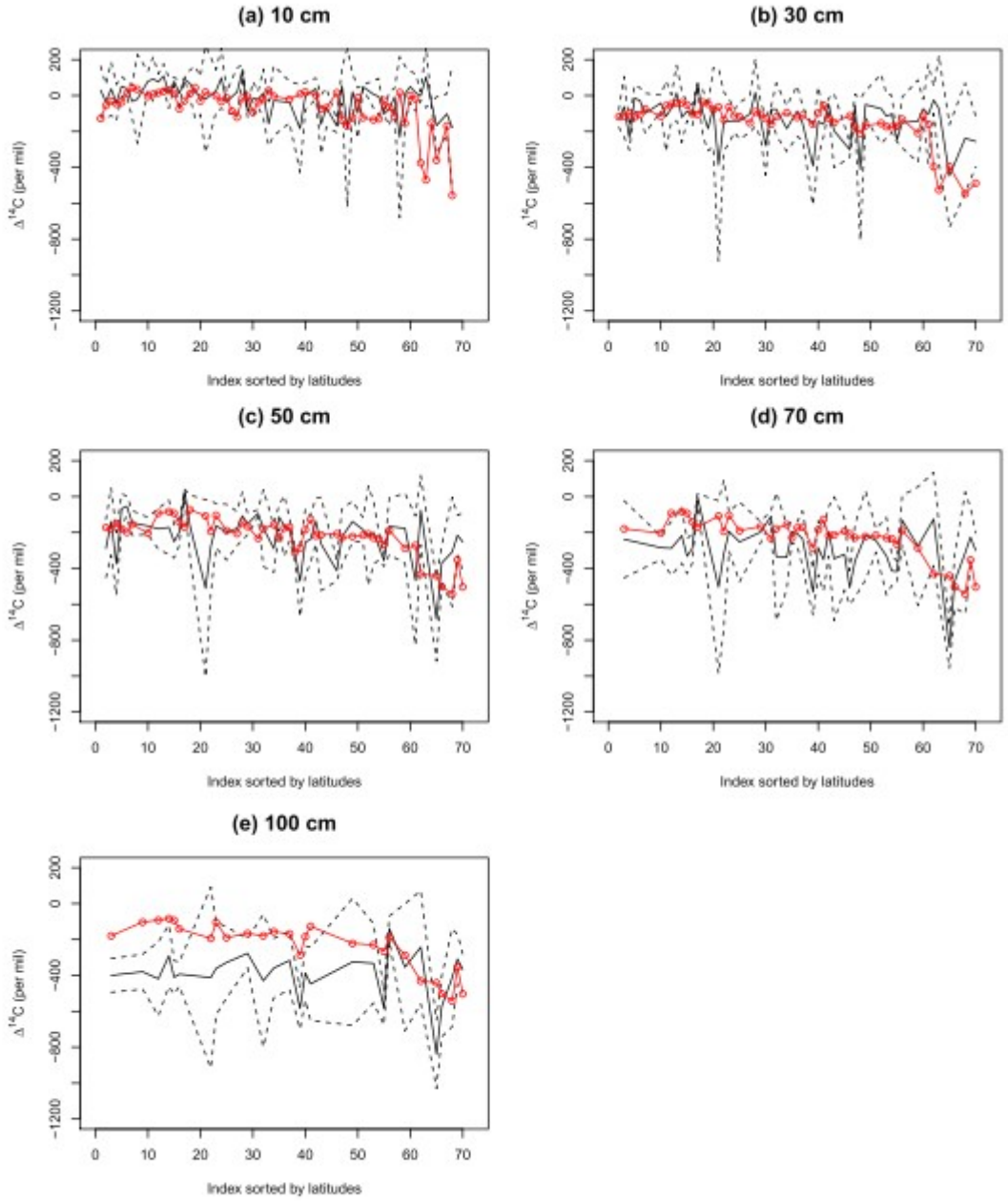

Figure 3. Comparison between mean observations (black curves) and ELMv1-ECA predictions (red curves) at 70 grid cells and depths of (a) 10 cm, (b) 30 cm, (c) 50 cm, (d) 70 cm, and (e) 100 cm. The black dashed lines show 95% bounds.

Figure 4 shows the vertical profiles of $\Delta^{14}C$ observations and model predictions to 100-cm depth within 21 grid cells across the globe where at least three observational sites with vertically resolved $\Delta^{14}C$ observations are available. Except for the three high-latitude grid cells (62, 65, and 68), the simulated near-surface (0–50 cm) SOC $\Delta^{14}C$ values all fall within, or are close to the 95% confidence bounds. The model captured the observed near-surface vertical $\Delta^{14}C$ profiles but consistently predicted too enriched $\Delta^{14}C$ values at depths >50 cm compared to the mean observed values.

Predictions were outside the 95% confidence bounds in seven of the grid cells at 100-cm depth (i.e., grid cells 3, 12, 15, 16, 39, 55, and 65).

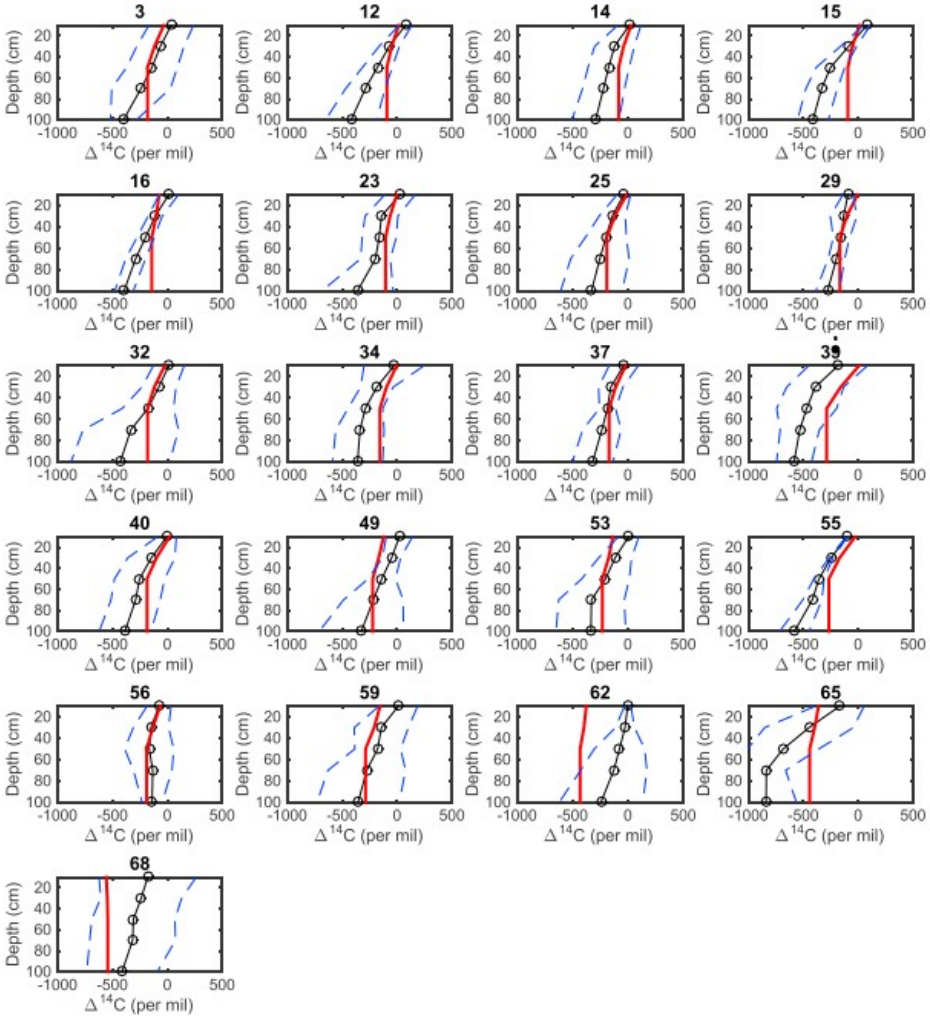

Figure 4. Comparison of vertical $\Delta^{14}C$ profiles for observed mean (black lines and symbols), observed 95% confidence bounds (blue dashed lines), and ELMv1-ECA predictions (red lines) for 21 grid cells, where at least three sites per grid cell had observations to 100-cm depth.

We also compared observed and predicted depth-resolved SOC stocks in 17 grid cells where at least three observational sites with vertically resolved observations to 100-cm depth are available (Figure 5). At depths of 10 and 30 cm, the model predictions were within or close to the 95% confidence bounds, except for grid cells 15, 16, 65, and 68. Generally, the predicted vertical profiles were less variable than observed, which we evaluated and improved in the site-level model simulations described below.

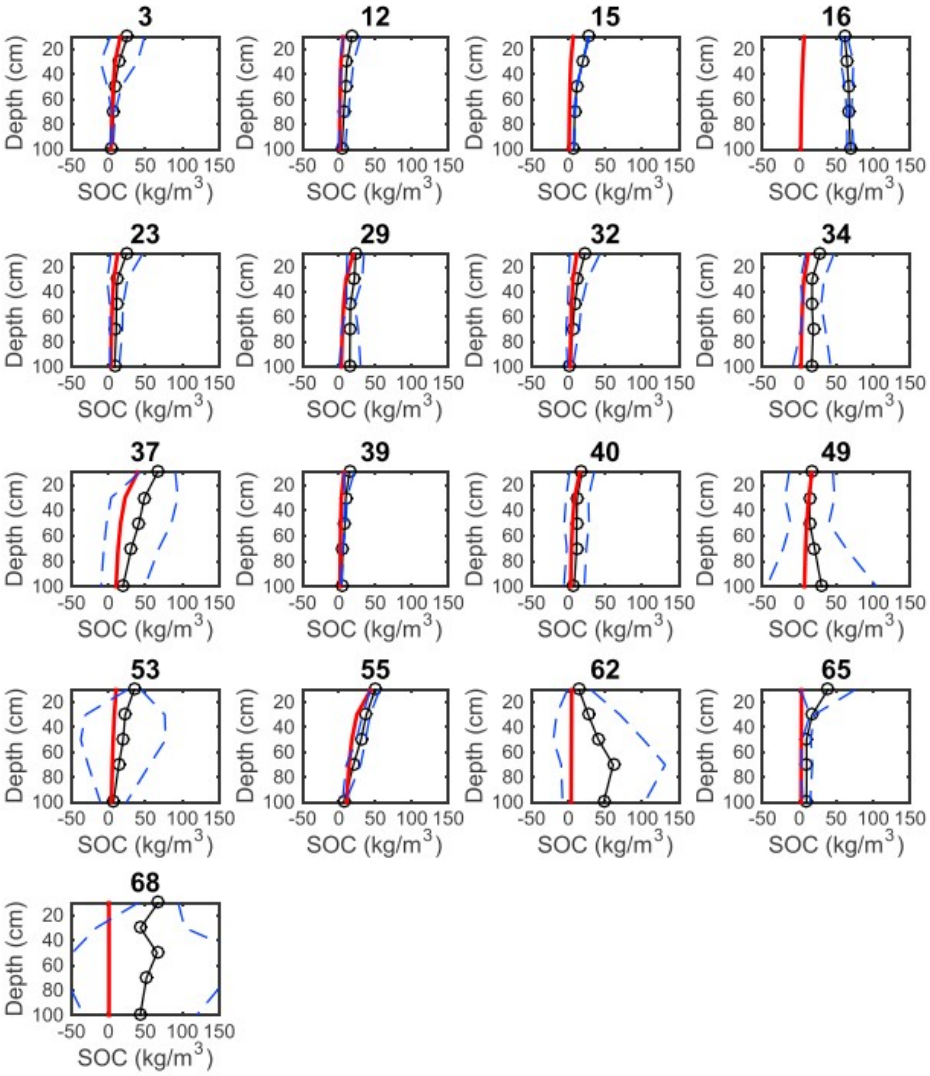

Figure 5. Comparison of vertical soil organic carbon (SOC) stock profiles for observed mean (black lines and symbols), observed 95% confidence bounds (blue dashed lines), and ELMv1-ECA predictions (red lines) for 17 grid cells, where at least three sites per grid cell had SOC stock observations to 100-cm depth.

3.2 Identification of Important Factors at the ESM Scale

We analyzed the limited $\Delta^{14}C$ observations using permutation-based hypothesis testing. Figure 6 shows the results obtained using random forests with 2,000 permutations. At 10-cm depth (Figure 6a), soil albedo index, soil order, slope, PFTs, SOM, and air temperature are important factors (i.e.,*p* values less than 0.10) for explaining discrepancies between observed and predicted $\Delta^{14}C$ values. At 30-cm depth (Figure 6b), soil albedo index, PFTs, and air temperature are among the most important factors. For deeper layers (i.e., 50, 70, and 100 cm; Figures 6c–6e), the only significant factors are SOM and PFTs.

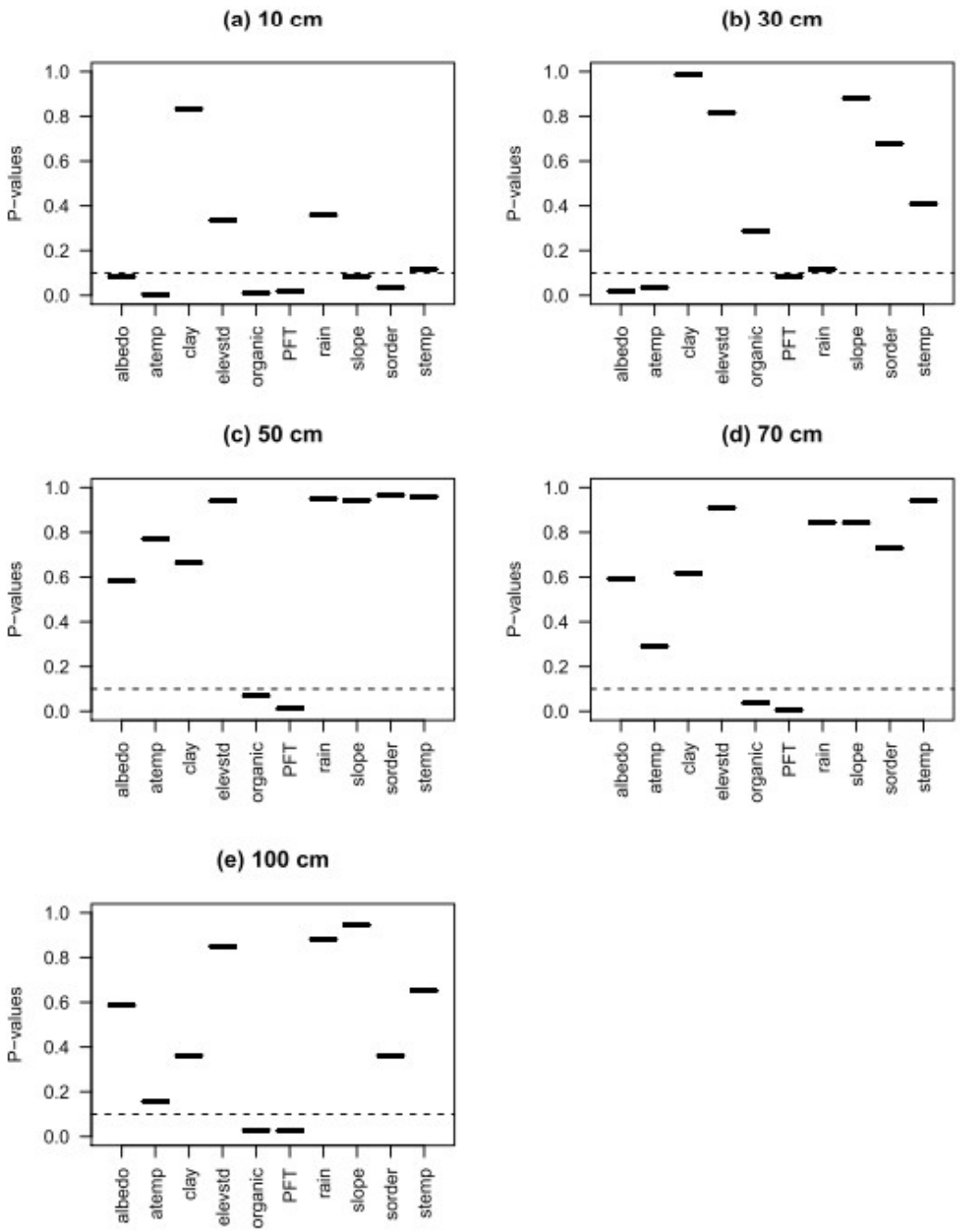

Figure 6. Importance ranking by permutation p values for depths (a) 10 cm, (b) 30 cm, (c) 50 cm, (d) 70 cm, and (e) 100 cm. The dashed line in each figure corresponds to the statistical significance level of 0.10. PFT = plant function type.

3.3 Sensitivity Analysis

To further investigate the capability of the model to reproduce the observed $\Delta^{14}C$ values and SOC content, we conducted sensitivity analysis with two rooting profiles (Jackson et al., 1997; Zeng, 2001) and five z_τ values, as described in section 2. Each of these simulations required a full spin-up, as described in section 2. We found that the model was highly sensitive to z_τ at

all five soil depths (10, 30, 50, 70, and 100 cm); deep soil predictions in many cases were also highly sensitive to the rooting profile (Figures 7 and 8). Importantly, no single z_τ parameter could reproduce the observations across all grid cells, which implied the importance of vertical differences in soil characteristics (e.g., soil microbial community, mineral protection, and root interaction) in determining soil decomposability.

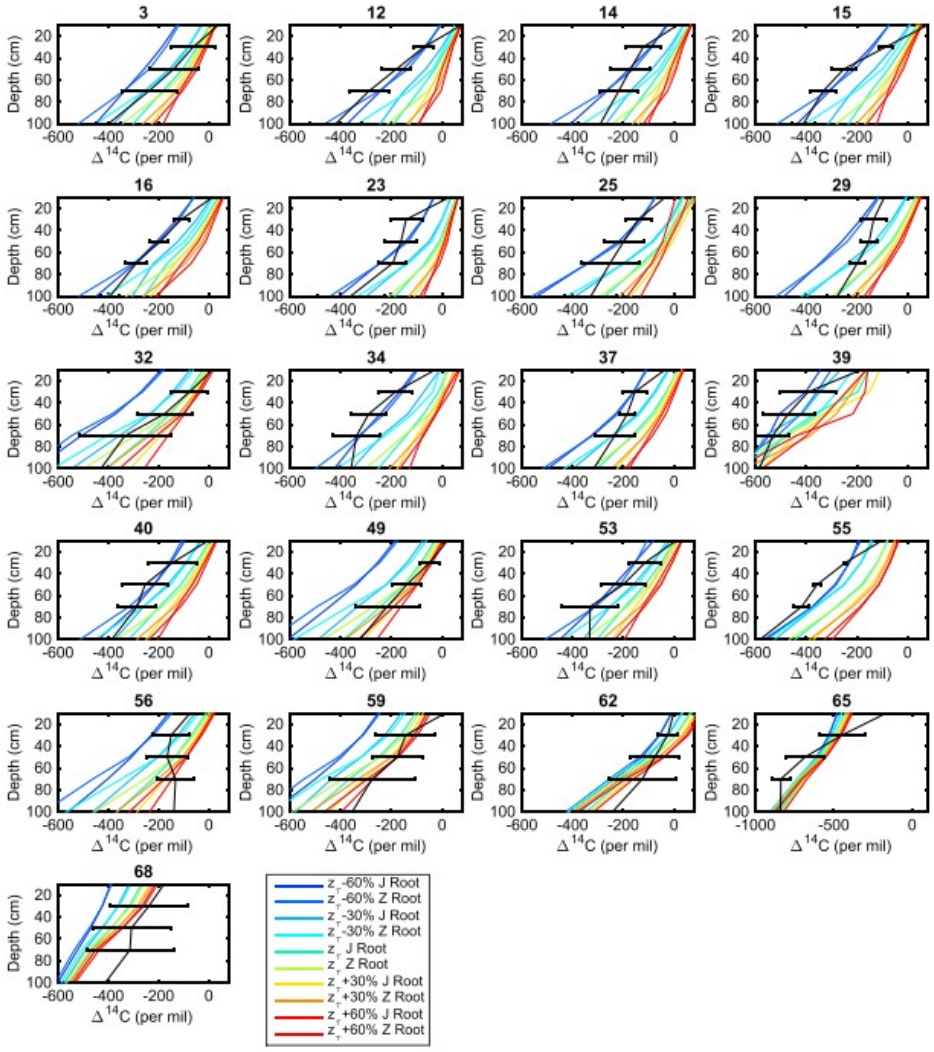

Figure 7. Ensemble simulation of ELMv1-ECA $\Delta^{14}C$ vertical profiles using different z_τ parameters (from −60% to +60% changes of the default value) and rooting profiles, where the Z root and J root refer to the rooting profiles from Zeng (2001) and Jackson et al. (1997). Black error bars represent observations and their 95% confidence intervals. Colored lines represent different ensembles, where warm color shows highest z_τ but cold color shows lowest z_τ.

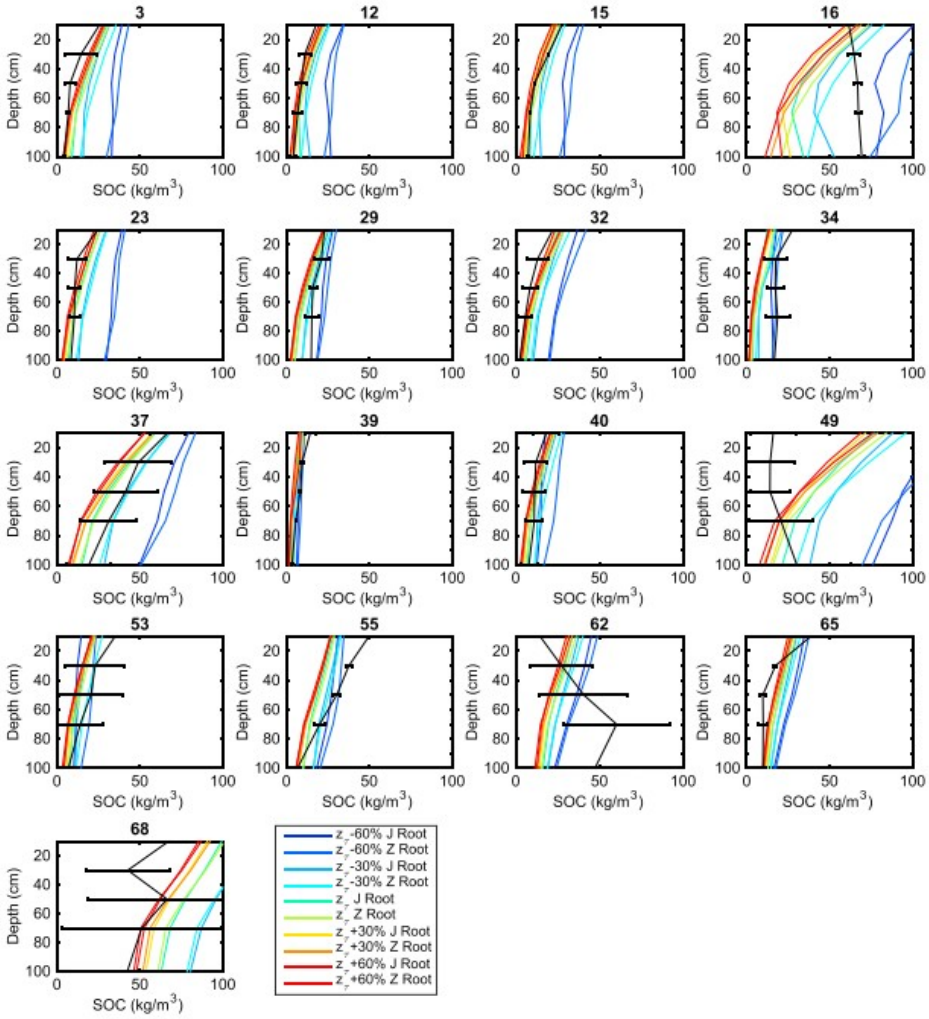

Figure 8. Ensemble simulation of ELMv1-ECA of soil organic carbon (SOC) vertical profiles using different z_τ parameters and rooting profiles. Note that four grid cells that have $\Delta^{14}C$ observations do not measure SOC. Black error bars represent observations and their 95% confidence intervals, and colored lines represent different ensembles.

We tested whether the discrepancies shown in Figures 7 and 8 can be reduced by adjusting rooting profiles and z_τ separately at the grid cell scale. The results (Figure 9) show that site-level parameter selections significantly reduced the differences between observed and predicted $\Delta^{14}C$ values and SOC content, highlighting the importance of site-level heterogeneity. Our results demonstrated that parameterization of soil carbon decomposability, especially in a vertically explicit matter, is challenging due to small-scale heterogeneity. A more mechanistic representation of soil decomposability is warranted in ESM land models, to accurately predict global soil carbon turnover, especially for deep soils.

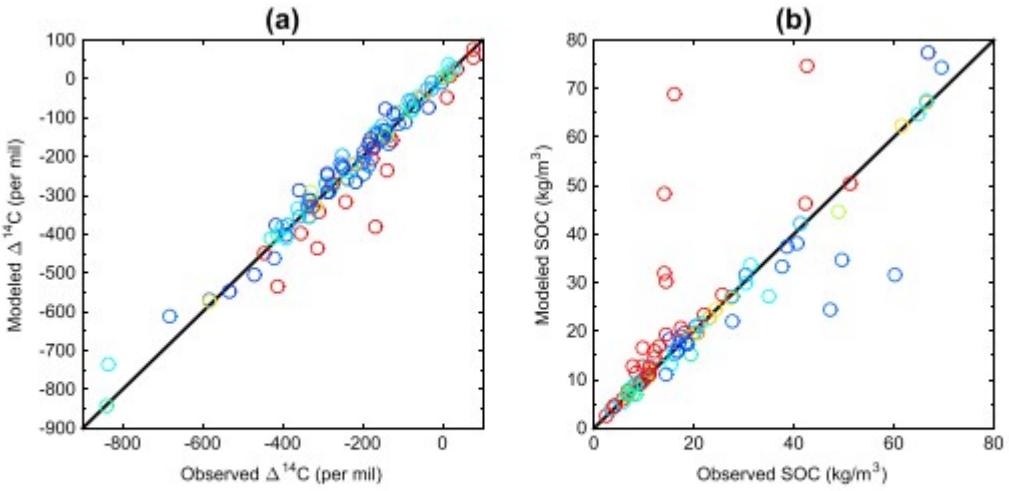

Figure 9. Model-data best fit using tuned site-specific z_r and rooting profiles for (a) $\Delta^{14}C$ profiles at 21 selected grid cells and (b) soil organic carbon (SOC) at 17 selected grid cells. Different color represents the same ensemble realizations as in Figures 7 and 8.

Contrary to expectations, $\Delta^{14}C$ predictions were more consistent with observations than SOC stocks (compare Figures 9a and 9b). Leaf litter inputs into soil concentrate in topsoil layers and requires vertical mixing to accumulate in deeper soil layers. In ELMv1-ECA, vertical mixing is parameterized as a diffusive flux with constant diffusivity across depth and sites. Fine root litter input to soil follows prescribed rooting profiles that decline with depth. In general, these two factors implicitly force higher predicted SOC content nearer the surface. In particular, the current model structure could not (regardless of parameter values) reproduce observed site-level SOC contents that increase with depth (e.g., Figure 8, sites 49 and 62; Figure 9 red outliers).

Since vertical diffusion of soil carbon could affect deep SOC stocks and $\Delta^{14}C$ values, we also conducted sensitivity analysis with vertical diffusion rates ranging from 0.0002 to 0.0008 m^2/year. We found that the predicted vertical $\Delta^{14}C$ profiles were less sensitive to vertical diffusion than to rooting profiles (see Figure 10). However, since it is widely recognized that model parameterization of vertical mixing is uncertain (Koven et al., 2013), we recommend that future work constrains these values observationally.

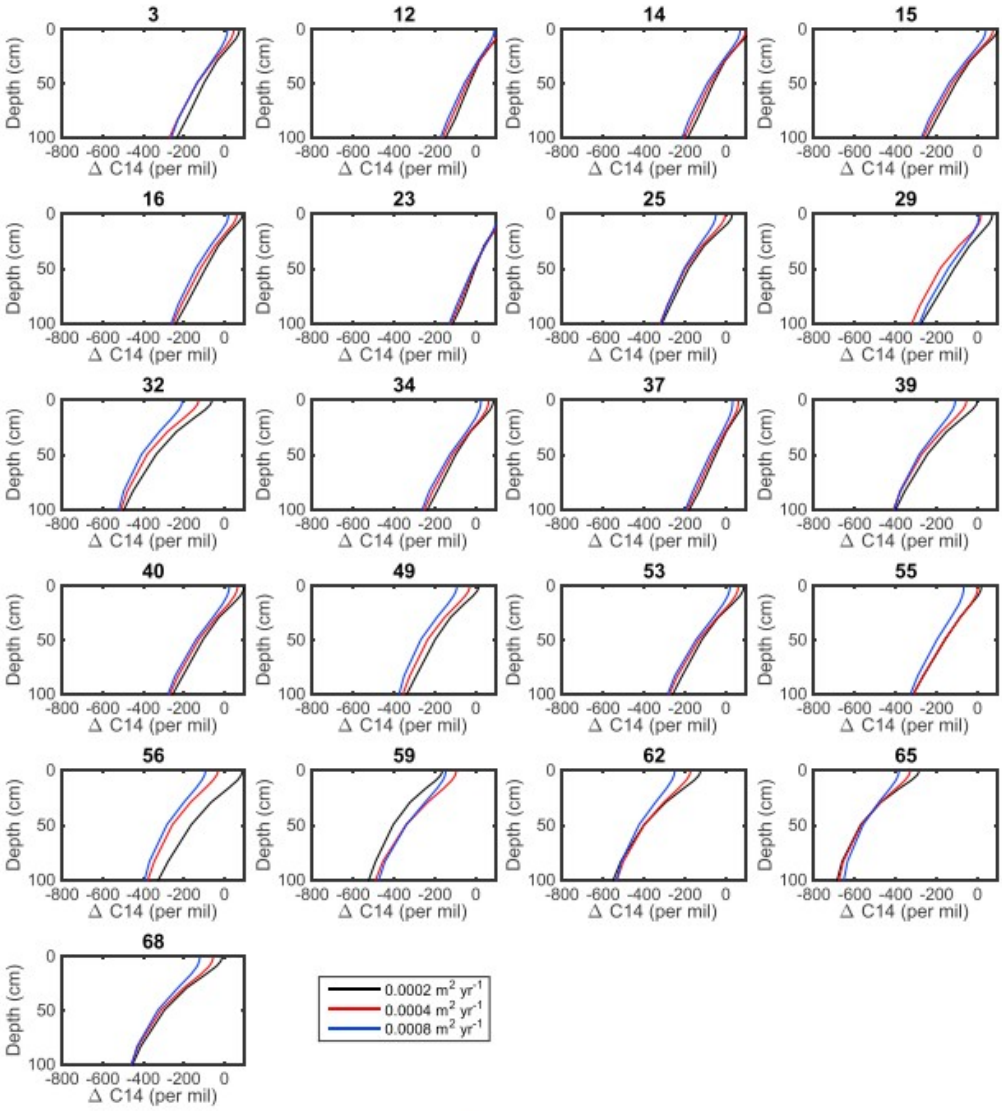

Figure 10. Model sensitivity analysis of how vertical diffusion rates affect $\Delta^{14}C$ profile.

4 Discussion

In this study, we evaluated soil carbon stock and turnover predictions from an ESM land model—ELMv1-ECA. Although direct comparisons between model predictions and mean site $\Delta^{14}C$ measurements at each depth were generally consistent, uncertainties in the averaged site measurements were large and their root mean square discrepancies with predictions increased with increasing depth (Figures 3 and 4). This result implied that parameterization of depth-dependent soil carbon turnover needs to be improved. In ELMv1-ECA, an exponential decay function (of soil depth) was applied (Koven et al., 2013), which was intended to represent the reduction of microbial activity with depth due to multiple unrepresented factors (e.g., physical protection and substrate supply). The larger model biases in deep soil toward younger soil carbon ages, compared with shallow soil, indicated

that this depth-dependent parameterization was oversimplified. As noted in section 2, the SOC $\Delta^{14}C$ bias associated with our assumption of a 0‰ atmosphere prior to the modern age may have led to biases between a few per mil near the surface and ~50‰ at depth. Such biases further motivate improved representation of processes leading to the observed vertical profiles of $\Delta^{14}C$ values and in particular to the relatively depleted values at depth.

Our sensitivity analysis revealed that the vertical decline of SOC decomposability with an *e*-folding factor in the model is insufficient (Figure 7). We argue that an improved model structure should be based on a mechanistic representation of plant, microbes, and mineral interactions, rather than a simple exponential decay factor. This argument is consistent with the results of several recent studies that use site-level land models and SOC and $\Delta^{14}C$ site observations. For example, Ahrens et al. (2015) used a process-based model (COMISSION) with the constraints from site-scale observations in Germany to study contribution of sorption, DOC transport, and microbial interactions to SOC $\Delta^{14}C$ profiles. They found different factors dominate SOC $\Delta^{14}C$ values in topsoil (≤30 cm; e.g., sorptive stabilization) and subsoil (>30 cm; e.g., DOC transport and microbial depolymerization). Dwivedi et al. (2017) used a biotic and abiotic model of SOM (i.e., BAMS1) and observations from a seven-site chronosequences in Northern California and from a Russian Chernozem site where soils were sampled 100 years apart. They demonstrated that explicitly incorporating microbial activity, sorption, and vertical transport led to consistent predictions of SOM stocks and $\Delta^{14}C$ values, with different dominant factors across the vertical profile. Our data-driven statistical analysis supports the idea that plants exert a strong control on SOC age, particularly in deep soils, but we note that we had insufficient site-level data to infer the relative strength of other potentially important factors, for example, vertical transport.

At the ESM scale and using machine learning-based analysis, we identified soil albedo index as one of the main factors at shallow depths (≤30 cm; Figure 6). As described by K. Oleson et al. (2013) in the technical description of CLM4.5, the soil albedo index was prescribed to best reproduce observed MODIS solar noon surface albedo values at the grid cell scale based on the method of Lawrence and Chase (2007). MODIS albedo is a compound variable dependent on many factors, such as solar zenith angles, surface soil moisture, fractional vegetation cover, leaf plus stem area index, and greenness (Liang et al., 2005; Myhre et al., 2005). Consequently, the soil albedo index used here is a compound factor representing a combination of multiple land surface features. The inferred strong relationship with SOC $\Delta^{14}C$ values may imply the importance of other grid cell-specific parameters not currently included in the model. This explanation is consistent with the very good predictions obtained when we applied grid cell-specific parameters to predict SOC stocks and $\Delta^{14}C$ values (Figure 9). Future work should identify

and quantify the controllers of these grid cell-specific parameters, which could then be used for extrapolation to larger scales.

PFT characterization played an important role in affecting the difference between the mean site measurements and ELMv1-ECA predictions. As shown in Figure 6, PFT was one of the most important factors for all depths. Similarly, SOMD was a very important factor in explaining differences between measured and simulated SOC $\Delta^{14}C$ values. The effects of soil order on SOC $\Delta^{14}C$ values are limited to the shallow subsurface (i.e., 10 cm) at the ESM scale. Soil order does not explain the mean measured data and their differences from ELMv1-ECA predictions beyond 10-cm depth (Figure 6).

There are several limitations related to acquisition and processing of soil radiocarbon measurements. First, soil radiocarbon data were primarily collected to enhance process understanding by maximizing differences of other factors (e.g., chronosequences), but not to characterize spatial variability at the ESM scale. These data were collected over many years by many investigators, and our approach here was to analyze that large existing ^{14}C data set. For the purpose of model comparison, ideally, sites would be selected so that the measured radiocarbon data have a better spatial representation of the entire grid cell. However, in practice, defining proper spatial representation for land modeling and for understanding terrestrial ecosystem dynamics remains a grand challenge.

Given current understanding of controllers on SOC stocks and $\Delta^{14}C$ values, we recommend future measurement campaigns additionally acquire information regarding, to the extent possible, plant properties (e.g., type, biomass, and rooting profiles) and soil properties (e.g., depth-resolved mineralogy and bulk density). Further, site selection should focus on characterizing spatial averages, rather than large gradients; observed quantities would facilitate development of quantities appropriate for comparison and analysis in an ESM context. Our analysis was driven and limited by quality and availability of other data types used at both ESM and site scales. It is therefore possible that we missed factors deemed to be important SOC decomposition controllers. In addition, the data set used for the current study was collected between 1900 and 2013; our model-based normalization to year 2000 (He et al., 2016) at each ESM grid cell could be subject to uncertainty.

Additionally, the current methods for calculating mean site measurements also suffered from limitations, such as small sample size. Currently, the sample size for grid cell-scale averaging was from 3 to 28, resulting in about 20–60% Monte Carlo errors. Moreover, we did not consider distance and spatial correlation structures in those site data. A straightforward but costly method to reduce uncertainty or errors is to collect significantly more site data. Another approach is to make strong assumptions on the spatial structure of soil $\Delta^{14}C$ values, for example, parametric models such as geostatistical methods (Cressie, 1993) or nonparametric models such as machine learning methods (Murphy, 2012). These types of methods are

typically applied to regional-scale problems, where other types of information may exist for deriving the spatial structure. Although current methods suffer from these limitations, to our knowledge, they are more realistic than traditional site- to ESM-scale comparisons.

5 Conclusions

We compared soil radiocarbon observations with a global land model (ELMv1-ECA, which is integrated in the ESM E3SM) at multiple depths through direct comparisons and through machine-learning analysis at the ESM grid cell scale. Using the same rooting depth parameter for each PFT and a single value for vertically resolved decomposition factor globally led to modeled SOC and $\Delta^{14}C$ values generally consistent with observations near the surface but with discrepancies increasing with depth. In general, the default model predicts too enriched $\Delta^{14}C$ values (i.e., too young SOC ages) at deeper depths. However, allowing grid cell-specific values for rooting and decomposition vertical profiles substantially improved model predictions compared to observations.

Our statistical analyses identified soil albedo index, PFTs, soil order, air temperature, and SOMD as the major factors with significant effects on predicting soil $\Delta^{14}C$ profiles at the ESM scale. However, these factors play different roles in shallow (≤30 cm) and deep (>30 cm) soils. The influences of soil albedo index, soil order, and air temperature on SOC and $\Delta^{14}C$ values were mainly limited to the shallow subsurface, but PFT and SOC density have effects on SOC $\Delta^{14}C$ values at all the depths.

Our study also suggested that we could reduce shallow-depth discrepancies between the observed and predicted large-scale $\Delta^{14}C$ values by using machine-learning methods and more accurate information regarding soil albedo index, soil order, and air temperature. However, to improve the predictions at deeper layers, better mechanistic models that describe SOC cycling rates and PFT effects are required. To this end, we tested the role of rooting profile, the *e*-folding factor controlling SOC decomposition depth dependence, and vertical diffusion rates. We found that a model that better captures factors controlling the depth dependence of microbial activity could improve $\Delta^{14}C$ predictions. Finally, we showed that site-specific values for rooting and decomposition vertical profiles substantially improved model predictions compared to observations. This latter result suggests that more site-specific information will be required to improve global-scale models of soil carbon cycling. Overall, our modeling and data analysis provide insights into the mechanisms that control observed patterns of soil $\Delta^{14}C$ profiles and thus provide useful guidance for future soil decomposition model development in ESM land models.

Acknowledgments

This research was supported by the RUBISCO SFA of the Regional and Global Modeling Analysis (RGMA) program and the ESM E3SM program in the

Climate and Environmental Sciences Division (CESD) of the Biological and Environmental Research (BER) Program in the U.S. Department of Energy Office of Science under contract DE-AC02-05CH11231. Dr. Susan Trumebore received financial support from the European Research Council through ERC-2015-AdG-695101. All data for the study are available at https://github.com/jschen83/Publication_Datasets.

References

Ahrens, B., Braakhekke, M. C., Guggenberger, G., Schrumpf, M., & Reichstein, M. (2015). Contribution of sorption, DOC transport and microbial interactions to the C-14 age of a soil organic carbon profile: Insights from a calibrated process model. *Soil Biology and Biochemistry*, 88, 390– 402. https://doi.org/10.1016/j.soilbio.2015.06.008

Archer, E. (2016), rfPermute: Estimate permutation p-values for random forests importance metrics, edited, R package version 2.1.5.

Bloom, A. A., Exbrayat, J. F., van derVelde, I. R., Feng, L., & Williams, M. (2016). The decadal state of the terrestrial carbon cycle: Global retrievals of terrestrial carbon allocation, pools, and residence times. *Proceedings of the National Academy of Sciences of the United States of America*, 113(5), 1285– 1290. https://doi.org/10.1073/pnas.1515160113

Breiman, L. (1996). Bagging predictors. *Machine Learning*, 24(2), 123– 140. https://doi.org/10.1007/BF00058655

Breiman, L. (2001). Random forests. *Machine Learning*, 45(1), 5– 32. https://doi.org/10.1023/A:1010933404324

Campo, J., & Merino, A. (2016). Variations in soil carbon sequestration and their determinants along a precipitation gradient in seasonally dry tropical forest ecosystems. *Global Change Biology*, 22(5), 1942– 1956. https://doi.org/10.1111/gcb.13244

Carvalhais, N., Forkel, M., Khomik, M., Bellarby, J., Jung, M., Migliavacca, M., Mu, M., Saatchi, S., Santoro, M., Thurner, M., Weber, U., Ahrens, B., Beer, C., Cescatti, A., Randerson, J. T., & Reichstein, M. (2014). Global covariation of carbon turnover times with climate in terrestrial ecosystems. *Nature*, 514(7521), 213– 217. https://doi.org/10.1038/nature13731

Cressie, N. A. C. (1993). *Statistics for spatial data*, Rev. Ed., Xx, 900 P. Pp. New York: Wiley.

Dwivedi, D., Riley, W. J., Torn, M. S., Spycher, N. F., Maggi, F., & Tang, J. Y. (2017). Mineral properties, microbes, transport, and plant-input profiles control vertical distribution and age of soil carbon stocks. *Soil Biology and Biochemistry*, 107, 244– 259. https://doi.org/10.1016/j.soilbio.2016.12.019

Efron, B., & Tibshirani, R. (1993). *An introduction to the bootstrap*, xvi, 436 p. pp. New York: Chapman & Hall. https://doi.org/10.1007/978-1-4899-4541-9

Friedlingstein, P., Joel, G., Field, C. B., & Fung, I. Y. (1999). Toward an allocation scheme for global terrestrial carbon models. *Global Change Biology*, 5(7), 755– 770. https://doi.org/10.1046/j.1365-2486.1999.00269.x

Friedlingstein, P., Meinshausen, M., Arora, V. K., Jones, C. D., Anav, A., Liddicoat, S. K., & Knutti, R. (2014). Uncertainties in CMIP5 climate projections due to carbon cycle feedbacks. *Journal of Climate*, 27(2), 511– 526. https://doi.org/10.1175/JCLI-D-12-00579.1

Ghimire, B., Riley, W. J., Koven, C. D., Mu, M. Q., & Randerson, J. T. (2016). Representing leaf and root physiological traits in CLM improves global carbon and nitrogen cycling predictions. *Journal of Advances in Modeling Earth Systems*, 8, 598– 613. https://doi.org/10.1002/2015MS000538

Harris, I., Jones, P. D., Osborn, T. J., & Lister, D. H. (2014). Updated high-resolution grids of monthly climatic observations—The CRU TS3.10 dataset. *International Journal of Climatology*, 34(3), 623– 642. https://doi.org/10.1002/joc.3711

Hastie, T., Tibshirani, R., & Friedman, J. H. (2009). *The elements of statistical learning: Data mining, inference, and prediction*, (2nd ed..xxii, 745 p. pp.). New York: Springer. https://doi.org/10.1007/978-0-387-84858-7

He, Y. J., Trumbore, S. E., Torn, M. S., Harden, J. W., Vaughn, L. J. S., Allison, S. D., & Randerson, J. T. (2016). Radiocarbon constraints imply reduced carbon uptake by soils during the 21st century. *Science*, 353(6306), 1419– 1424. https://doi.org/10.1126/science.aad4273

Hengl, T., deJesus, J. M., MacMillan, R. A., Batjes, N. H., Heuvelink, G. B. M., Ribeiro, E., Samuel-Rosa, A., Kempen, B., Leenaars, J. G. B., Walsh, M. G., & Gonzalez, M. R. (2014). SoilGrids1km—Global soil information based on automated mapping. *PLoS ONE*, 9(8), e105992. https://doi.org/10.1371/journal.pone.0105992

Jackson, R. B., Mooney, H. A., & Schulze, E. D. (1997). A global budget for fine root biomass, surface area, and nutrient contents. *Proceedings of the National Academy of Sciences*, 94(14), 7362– 7366. https://doi.org/10.1073/pnas.94.14.7362

Jenkinson, D. S., & Coleman, K. (2008). The turnover of organic carbon in subsoils. Part 2. Modelling carbon turnover. *European Journal of Soil Science*, 59(2), 400– 413. https://doi.org/10.1111/j.1365-2389.2008.01026.x

Jiang, L. F., Yan, Y. E., Hararuk, O., Mikle, N., Xia, J. Y., Shi, Z., Tjiputra, J., Wu, T. W., & Luo, Y. Q. (2015). Scale-dependent performance of CMIP5 earth system models in simulating terrestrial vegetation carbon. *Journal of Climate*, 28(13), 5217– 5232. https://doi.org/10.1175/JCLI-D-14-00270.1

Klueter, A., Crandall, J. B., Archer, F. I., Teece, M. A., & Coffroth, M. A. (2015). Taxonomic and environmental variation of metabolite profiles in

marine dinoflagellates of the genus symbiodinium. *Metabolites*, 5(1), 74– 99. https://doi.org/10.3390/metabo5010074

Koven, C. D., Riley, W. J., Subin, Z. M., Tang, J. Y., Torn, M. S., Collins, W. D., Bonan, G. B., Lawrence, D. M., & Swenson, S. C. (2013). The effect of vertically resolved soil biogeochemistry and alternate soil C and N models on C dynamics of CLM4. *Biogeosciences*, 10(11), 7109– 7131. https://doi.org/10.5194/bg-10-7109-2013

Lamarque, J. F., Kiehl, J. T., Brasseur, G. P., Butler, T., Cameron-Smith, P., Collins, W. D., Collins, W. J., Granier, C., Hauglustaine, D., Hess, P. G., & Holland, E. A. (2005). Assessing future nitrogen deposition and carbon cycle feedback using a multimodel approach: Analysis of nitrogen deposition. *Journal of Geophysical Research*, 110, D19303. https://doi.org/10.1029/2005JD005825

Lawrence, P. J., & Chase, T. N. (2007). Representing a new MODIS consistent land surface in the Community Land Model (CLM 3.0). *Journal of Geophysical Research*, 112, G01023. https://doi.org/10.1029/2006JG000168

Lawrence, P. J., & Chase, T. N. (2010). Investigating the climate impacts of global land cover change in the Community Climate System Model. *International Journal of Climatology*, 30(13), 2066– 2087. https://doi.org/10.1002/joc.2061

Levin, I., Naegler, T., Kromer, B., Diehl, M., Francey, R. J., Gomez-Pelaez, A. J., Steele, L. P., Wagenbach, D., Weller, R., & Worthy, D. E. (2010). Observations and modelling of the global distribution and long-term trend of atmospheric (CO_2)-C-14 (vol 62, pg 26, 2010). *Tellus B*, 62(3), 207– 207.

Liang, Y. K., Dubos, C., Dodd, I. C., Holroyd, G. H., Hetherington, A. M., & Campbell, M. M. (2005). AtMYB61, an R2R3-MYB transcription factor controlling stomatal aperture in *Arabidopsis thaliana*. *Current Biology*, 15(13), 1201– 1206. https://doi.org/10.1016/j.cub.2005.06.041

Liski, J., Lehtonen, A., Palosuo, T., Peltoniemi, M., Eggers, T., Muukkonen, P., & Makipaa, R. (2006). Carbon accumulation in Finland's forests 1922–2004—An estimate obtained by combination of forest inventory data with modelling of biomass, litter and soil. *Annals of Forest Science*, 63(7), 687– 697. https://doi.org/10.1051/forest:2006049

Luo, Y. Q., Ahlström, A., Allison, S. D., Batjes, N. H., Brovkin, V., Carvalhais, N., Chappell, A., Ciais, P., Davidson, E. A., Finzi, A., & Georgiou, K. (2016). Toward more realistic projections of soil carbon dynamics by Earth system models. *Global Biogeochemical Cycles*, 30, 40– 56. https://doi.org/10.1002/2015GB005239

Mahowald, N., Jickells, T. D., Baker, A. R., Artaxo, P., Benitez-Nelson, C. R., Bergametti, G., Bond, T. C., Chen, Y., Cohen, D. D., Herut, B., Kubilay, N., Losno, R., Luo, C., Maenhaut, W., McGee, K. A., Okin, G. S., Siefert, R. L., & Tsukuda, S. (2008). Global distribution of atmospheric phosphorus sources, concentrations and deposition rates, and anthropogenic impacts. *Global Biogeochemical Cycles*, 22, GB4026. https://doi.org/10.1029/2008GB003240

Masarie, K. A., & Tans, P. P. (1995). Extension and integration of atmospheric carbon-dioxide data into a globally consistent measurement record. *Journal of Geophysical Research*, 100(D6), 11593– 11,610. https://doi.org/10.1029/95JD00859

Mathieu, J. A., Hatte, C., Balesdent, J., & Parent, E. (2015). Deep soil carbon dynamics are driven more by soil type than by climate: A worldwide meta-analysis of radiocarbon profiles. *Global Change Biology*, 21(11), 4278– 4292. https://doi.org/10.1111/gcb.13012

Mekonnen, Z. A., Grant, R. F., & Schwalm, C. (2016). Sensitivity of modeled NEP to climate forcing and soil at site and regional scales: Implications for upscaling ecosystem models. *Ecological Modelling*, 320, 241– 257. https://doi.org/10.1016/j.ecolmodel.2015.10.004

Mishra, U., & Riley, W. J. (2015). Scaling impacts on environmental controls and spatial heterogeneity of soil organic carbon stocks. *Biogeosciences*, 12(13), 3993– 4004. https://doi.org/10.5194/bg-12-3993-2015

Murphy, K. P. (2012). *Machine learning: A probabilistic perspective*, xxix, 1067 pp. Cambridge, MA: MIT Press.

Myhre, G., Kvalevag, M. M., & Schaaf, C. B. (2005). Radiative forcing due to anthropogenic vegetation change based on MODIS surface albedo data. *Geophysical Research Letters*, 32, L21410. https://doi.org/10.1029/2005GL024004

Oleson, K., Lawrence, D. M., Bonan, G. B., Drewniak, B., Huang, M., Koven, C. D., Levis, S., Li, F., Riley, W. J., Subin, Z. M., Swenson, S., Thornton, P. E., Bozbiyik, A., Fisher, R., Heald, C. L., Kluzek, E., Lamarque, J.-F., Lawrence, P. J., Leung, L. R., Lipscomb, W., Muszala, S. P., Ricciuto, D. M., Sacks, W. J., Sun, Y., Tang, J., &Yang, Z.-L. (2013). Technical description of version 4.5 of the Community Land Model (CLM), *NCAR Technical Note NCAR/TN-503+STR*, 420 pp. https://doi.org/10.5065/D6RR1W7M

Oleson, K. W., & Bonan, G. B. (2000). The effects of remotely sensed plant functional type and leaf area index on simulations of boreal forest surface fluxes by the NCAR land surface model. *Journal of Hydrometeorology*, 1(5), 431– 446. https://doi.org/10.1175/1525-7541(2000)001<0431:TEORSP>2.0.CO;2

Parton, W. J., Scurlock, J. M. O., Ojima, D. S., Gilmanov, T. G., Scholes, R. J., Schimel, D. S., Kirchner, T., Menaut, J. C., Seastedt, T., Garcia Moya,

E., Kamnalrut, A., & Kinyamario, J. I. (1993). Observations and modeling of biomass and soil organic-matter dynamics for the grassland biome worldwide. *Global Biogeochemical Cycles*, 7(4), 785– 809. https://doi.org/10.1029/93GB02042

Reimer, P. J., Bard, E., Bayliss, A., Beck, J. W., Blackwell, P. G., Ramsey, C. B., Buck, C. E., Cheng, H., Edwards, R. L., Friedrich, M., Grootes, P. M., Guilderson, T. P., Haflidason, H., Hajdas, I., Hatté, C., Heaton, T. J., Hoffmann, D. L., Hogg, A. G., Hughen, K. A., Kaiser, K. F., Kromer, B., Manning, S. W., Niu, M., Reimer, R. W., Richards, D. A., Scott, E. M., Southon, J. R., Staff, R. A., Turney, C. S. M., & van derPlicht, J. (2013). Intcal13 and Marine13 radiocarbon age calibration curves 0–50,000 years cal BP. *Radiocarbon*, 55(04), 1869– 1887. https://doi.org/10.2458/azu_js_rc.55.16947

Riley, W. J., Maggi, F., Kleber, M., Torn, M. S., Tang, J. Y., Dwivedi, D., & Guerry, N. (2014). Long residence times of rapidly decomposable soil organic matter: Application of a multi-phase,multi-component, and vertically resolved model (BAMS1) to soil carbon dynamics. *Geoscientific Model Development*, 7(4), 1335– 1355. https://doi.org/10.5194/gmd-7-1335-2014

Riley, W. J., Zhu, Q., & Tang, J. Y. (2018). Weaker land–climate feedbacks from nutrient uptake during photosynthesis-inactive periods. *Nature Climate Change*, 8(11), 1002– 1006. https://doi.org/10.1038/s41558-018-0325-4

Schmidt, M. W. I., Torn, M. S., Abiven, S., Dittmar, T., Guggenberger, G., Janssens, I. A., Kleber, M., Kögel-Knabner, I., Lehmann, J., Manning, D. A. C., Nannipieri, P., Rasse, D. P., Weiner, S., & Trumbore, S. E. (2011). Persistence of soil organic matter as an ecosystem property. *Nature*, 478(7367), 49– 56. https://doi.org/10.1038/nature10386

Schrumpf, M., Schulze, E. D., Kaiser, K., & Schumacher, J. (2011). How accurately can soil organic carbon stocks and stock changes be quantified by soil inventories?*Biogeosciences*, 8(5), 1193– 1212. https://doi.org/10.5194/bg-8-1193-2011

Schwalm, C. R., Williams, C. A., Schaefer, K., Anderson, R., Arain, M. A., Baker, I., Barr, A., Black, T. A., Chen, G., Chen, J. M., Ciais, P., Davis, K. J., Desai, A., Dietze, M., Dragoni, D., Fischer, M. L., Flanagan, L. B., Grant, R., Gu, L., Hollinger, D., Izaurralde, R. C., Kucharik, C., Lafleur, P., Law, B. E., Li, L., Li, Z., Liu, S., Lokupitiya, E., Luo, Y., Ma, S., Margolis, H., Matamala, R., McCaughey, H., Monson, R. K., Oechel, W. C., Peng, C., Poulter, B., Price, D. T., Riciutto, D. M., Riley, W., Sahoo, A. K., Sprintsin, M., Sun, J., Tian, H., Tonitto, C., Verbeeck, H., & Verma, S. B. (2010). A model-data intercomparison of CO_2 exchange across North America: Results from the North American Carbon Program site synthesis. *Journal of Geophysical Research*, 115, G00H05. https://doi.org/10.1029/2009JG001229

Tang, J., & Riley, W. (2013). A total quasi-steady-state formulation of substrate uptake kinetics in complex networks and an example application to microbial litter decomposition. *Biogeosciences*, 10(12), 8329– 8351. https://doi.org/10.5194/bg-10-8329-2013

Task, G. S. D. (2000), Global data products CD-ROM (IGBP-DIS), *CD-ROM. International Geosphere-Biosphere Programme, Data and Information System, Potsdam, Germany. Available from Oak Ridge National Laboratory Distributed Active Archive Center, Oak Ridge, Tennessee, U.S.A*. [http://www.daac.ornl.gov]

Thomsen, I. K., Schjonning, P., Olesen, J. E., & Christensen, B. T. (2003). C and N turnover in structurally intact soils of different texture. *Soil Biology and Biochemistry*, 35(6), 765– 774. https://doi.org/10.1016/S0038-0717(03)00093-2

Torn, M. S., Trumbore, S. E., Chadwick, O. A., Vitousek, P. M., & Hendricks, D. M. (1997). Mineral control of soil organic carbon storage and turnover. *Nature*, 389(6647), 170– 173. https://doi.org/10.1038/38260

Verdin, K. L., & Greenlee, S. K. (1996). *Development of continental scale digital elevation models and extraction of hydraugraphic features, Proceedings of Third International Conference/Workshop on Integrating GIS and Environmental Modeling, Sante Fe, New Mexico*, January 21–26. Santa Barbara, Calif: Natl. Cent. for Geogr. Inf. and Anal.

Viovy, N. (2018). *CRUNCEP version 7—Atmospheric forcing data for the Community Land Model*. Research Data Archive at the National Center for Atmospheric Research. Boulder CO, USA: Computational and Information Systems Laboratory.

Walker, A. P., Beckerman, A. P., Gu, L. H., Kattge, J., Cernusak, L. A., Domingues, T. F., Scales, J. C., Wohlfahrt, G., Wullschleger, S. D., & Woodward, F. I. (2014). The relationship of leaf photosynthetic traits—V_{cmax} and J_{max}—to leaf nitrogen, leaf phosphorus, and specific leaf area: A meta-analysis and modeling study. *Ecology and Evolution*, 4(16), 3218– 3235. https://doi.org/10.1002/ece3.1173

Wang, Y. P., Houlton, B. Z., & Field, C. B. (2007). A model of biogeochemical cycles of carbon, nitrogen, and phosphorus including symbiotic nitrogen fixation and phosphatase production. *Global Biogeochemical Cycles*, 21, GB1018. https://doi.org/10.1029/2006GB002797

Zeng, X. B. (2001). Global vegetation root distribution for land modeling. *Journal of Hydrometeorology*, 2(5), 525– 530. https://doi.org/10.1175/1525-7541(2001)002<0525:GVRDFL>2.0.CO;2

Zhu, Q., Riley, W., & Tang, J. (2017). A new theory of plant–microbe nutrient competition resolves inconsistencies between observations and model

predictions. *Ecological Applications*, 27(3), 875– 886. https://doi.org/10.1002/eap.1490

Zhu, Q., Riley, W., Tang, J., & Koven, C. (2016). Multiple soil nutrient competition between plants, microbes, and mineral surfaces: Model development, parameterization, and example applications in several tropical forests. *Biogeosciences*, 13(1), 341– 363. https://doi.org/10.5194/bg-13-341-2016